International Journal of Electrical Components and Energy Conversion
2015; 1(1): 24-35
Published online March 31, 2015 (http://www.sciencepublishinggroup.com/j/ijecec)
doi: 10.11648/j.ijecec.20150101.13

Optimal Design and Control of Electric Vehicles Power Chain with Electromagnetic Switch

Mariem Ben Amor[1], Ajmia Belgacem[2], Souhir Tounsi[3]

[1]National School of Engineers of Sfax (ENIS), Sfax University, SETIT Research Unit, Sfax, Tunisia
[2]National School of Engineers of Gabès (ENIG), Gabès University, SETIT Research Unit, Sfax, Tunisia
[3]National School of Electronics and Telecommunications of Sfax, Sfax University, SETIT Research Unit, Sfax, Tunisia

Email address:
souhir.tounsi@enetcom.rnu.tn (S. Tounsi)

To cite this article:
Mariem Ben Amor, Ajmia Belgacem, Souhir Tounsi. Optimal Design and Control of Electric Vehicles Power Chain with Electromagnetic Switch. *International Journal of Electrical Components and Energy Conversion.* Vol. 1, No. 1, 2015, pp. 24-35.
doi: 10.11648/j.ijecec.20150101.13

Abstract: In this paper, we present an analytical approach to design of the power train of electric vehicles. This approach is based on the application of general theorems relating to the design of an electrical device, such as amper theorem. This design method provides results of power chain manufacturing, quickly and without iterations. It is compatible concequently to optimization approaches, such as performance of the motor-converter. A validation study of the design approach by the finite element method is also presented. A comparative study between a power chain to trapezoidal control and another to sinusoidal control is presented.

Keywords: Power Chain, Analytic Method, Sizing, Electric Motor, Electromagnetic Switches Converter

1. Introduction

In this paper, we present a methodology for a systematic design of the power train of electric vehicles (EVs), taking into account of several constraints such as the speed limit, the energy savings, the cost of the power chain and the reliability of the overall system. This methodology is based on one hand on the dimensioning of the analytical power chain, and secondly on the analytical model of the electrical and control parameters of the electric actuator. This methodology takes into account the compatibility between the components of the power chain to achieve the critical level of performance of the overall system. This approach is based on the application of general theorems relating to the design of electrical devices. The overall design model provides results of manufacturing of the electric motor, the converter and the mechanical transmission system quickly and without iterations [1]. This feature increases the compatibility of this approach to procedures optimizing the performance of EVs, such as speed limit, autonomy, and cost of production.

To broaden the search range of effective solutions solving the problem of electric traction, two types of alternative converters are used to drive EVs at variable speed:

- The converter with IGBT strongly addressed in the literature [2] and [3].
- The converter with electromagnetic switches (IEs), which we detail the design approach and the modeling of magnetic and electrical parameters.

In this context, four structures of traction motor that may arise following nine configurations with the same stator are defined.

A validation and complementarily study by the finite element method to adjust the design process is developped and presented. Finally a comparative study between the power chain to trapezoidal control and the other to sinusoidal control is presented.

The systematic design approach developed presents a design tool of EVs power chains.

2. Power Chain Structure

Several configurations of power chain are shown in the literature. We cite as examples:

- The four-engine wheels configuration to direct mechanical linkage or gears.
- The configuration with two motors front or rear to direct

connection or with gear.

- The single-engine configuration with mechanical differential transmission more gears or gearless. This configuration is chosen for our application because it offers the advantage of low cost, because the manufacture of a single motor is less expensive than many engines [3-10]. This configuration also avoids the problem of slippage since it is impossible to control several motors at the same speed.

2.1. Principle of Functioning

The schematic structure of the power train is illustrated in Figure 1 [5] and [6].

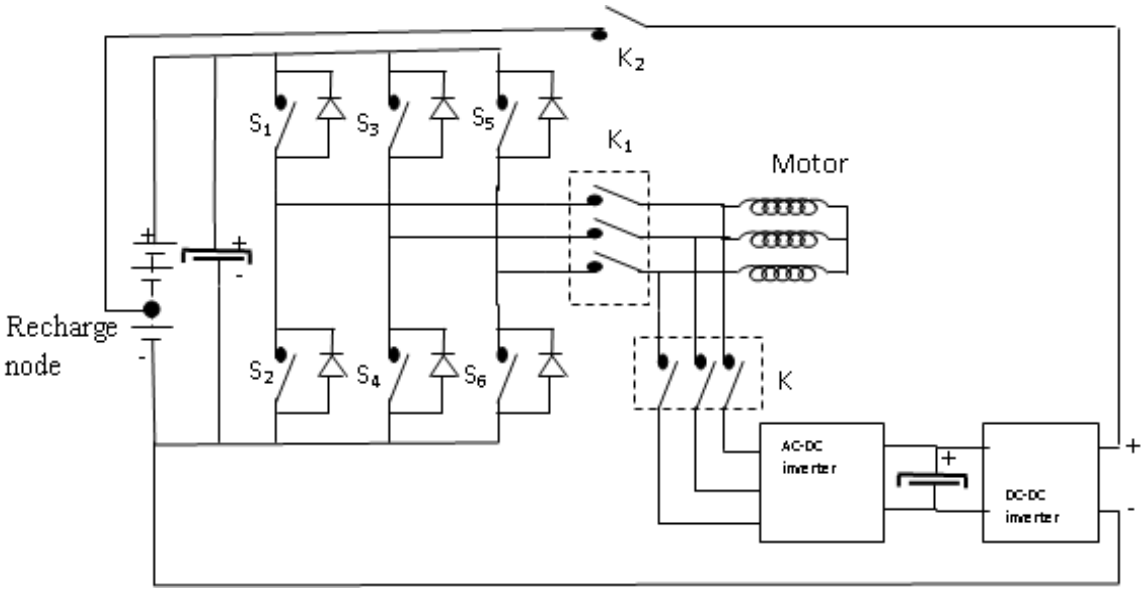

Figure 1. *Power chain structure.*

During the phases of acceleration and operation at constant speed, the motor is driven by the static electromagnetic switch converter according to a vector control strategy fixing the motor phase current in phase with the electromotive force, leading to a minimization of energy consumption. In this case the switches K and K2 are open, by action of their control generator coils. As against, during deceleration phases for a recoverable energy, K1 is opened and K, K2 are closed which causes the operation of the energy recovery system. In this case the motor operates as a generator. Indeed, the three electromotive forces induced by inertial force of the vehicle is transformed into a DC voltage elevated by a DC-DC elevator converter with a cycle ratio optimized in order to maximize the energy recovered by the accumulator of energy. This voltage is applied to the battery at charging node. This node is selected in a way to maximize the energy recovered [6-13].

2.2. Static Converter Structure

The static converter is a two-level inverter voltage. This structure is the least expensive compared to others and offers good quality of voltages and currents wave-forms, which leads to a good dynamic characteristic of EVs. Two inverter types are studied, the IGBT converter structure and the electromagnetic switches converetr strucure (IEs). The latter structure has the disadvantage of low switching frequency (Below 150 Hz), but it is less expensive and does not pose the problem of floating potential, since each inverter arm is controlled by a single electro-magnet. Against, the IGBT structure offers the possibility to achieve a switching frequency of 8000 Hz which leads to a good quality of the dynamic characteristic of EVs, it present a lot of disadvantages which can be cited as examples :

- Energy losses leading to a reduced range for a stored energy also establishes the temperature rise in the transistors and diodes leading to the incorporation of a cooling system in most cases .

- The problem of potential-floating leading to a complication of the electronic control circuit.
- The intervention of capacity Trigger-Source, Trigger-Drain and Drain-Source. These capabilities occur especially at high frequencies leading to a deterioration of the quality of control signals and subsequently to performance degradation of the overall drive system
- The problem of static and dynamic Luch-up generally leading to the deterioration of the converter. In this paper we only present the design process of the converter with electromagnetic switches (IEs). Design methods of the IGBT inverter are highly processed and presented in the literature.

2.3. Electric Motor Configurations

2.3.1. Criteria for Configurations Selecting

The sought-after configurations must be to reduced manufacture cost and elevated power to weight ratio. They must be modular (with multi-stages) to cover a large beach of power and to reduce the maintenance cost. In this context we keep axial structures, to open and right slots reducing the cost

of manufacture and maintenance. The chosen coil is concentrated (every coil is rolled up around a tooth), facilitating its insertion around the stator teeth. The concentrated winding present the advantage of its insertion in only one block, what facilitates the automation of the production procedure in big sets. The concentrated winding also leads to the reduction of the end winding.

To widen the beach of research, we keep some synchronous configurations of electric motor to permanent magnet (MSAP). These structures are equivalent of point of view power and shapes of waves.

2.3.2. Found Configurations

Research is spread to triphase structures to permanent magnets, to coiled rotor and to double excitation. These structures are either to sinusoïdal or trapezoidal shape of wave according to the rules of optimization respecting the criterias of configurations choice:

1. for structures to trapezoidal shape of wave, the angular width of a magnet (or of the opening of coil for the structures to coiled rotor and the structures to double excitation) is equal to the polar step, while for a structure to sinusoidal shape of wave, the angular width of the magnet (or of the opening of the coil for the structures to coiled rotor and the structures to double excitation) is equal to the polar step or to 3/2 the polar step.

2. the angular width of the magnets (or of the opening of the coil for the structures to coiled rotor and the structures to double excitation) is equal to the angular width of the teeth for structures to trapezoidal shape of wave, while 3/2 of the width of the teeth for structures to sinusoidal shape of wave

3. every slots contains two sides of coils and an inserted tooth.

4. all coils have the same shape, as well as all stator teeth and the inserted teeth.

5. the winding of a phase is gotten in series by the stake of several coils.

6. positioning of the coils to have electromotive forces schifted of 2 /3.π.

7. reversing the direction of winding in the case where a coil is opposite a south magnet instead of being in front of a north magnet and vice versa.

The inserted teeth intervene if the surface of the teeth in front of the magnets to North Pole is not equal to the surface of the teeth in front of the magnets in some south pole either the position of rotor. If it is true, the inserted teeth permit to have a trapezoidal shape of the electromotive force.

9 configurations obeying these rules are found, each of which is characterized by an variation law of the number of pole pairs p as a function of an integer n variant between 1 and to infinite , the ratio of main teeth N_d by the number of pole pairs p denoted r , the ratio ν of the angular width between the two main teeth and a main tooth , the ratio α between the angular width of a main tooth and that of a magnet (or the opening of the coil for the wound rotor and double excitation structures) and the ratio β of the angular width of a magnet (or the opening of the coil for the wound rotor and double excitation structures) and the pole pitch .

For structures with parallel excitation, the dimensions and the position of the two magnets inserted on either side of the axis of the electromagnet are calculated so as to have the same electric constant of the electromotive force.

Table 1 gives these reports for four sinusoidal configurations and five trapezoidal configurations [7].

Table 1. *Found configurations.*

Sinusoidal configurations	p	r	ν	α	β	Trapezoidal configurations	p	r	ν	α	β
1	2.n	1.5	1	2/3	1	1	2.n	1.5	1/3	1	1
2	5.n	1.2	3/2	2/3	1	2	5.n	1.2	2/3	1	1
3	2.n	1.5	1/3	3/2	2/3	3	7.n	6/7	4/3	1	1
4	5.n	1.2	2/3	3/2	2/3	4	4.n	0.75	5/3	1	1
						5	5.n	0.6	7/3	1	1

on to the motor working in its environment. To remedy this problem, we reversed the sense of resolution of the problem completely, while leaving from the need (Torque, strength of attraction, speed for the whole motor converter) toward the geometric measurements. It is necessary to recognize also that the inversion of the problem facilitates the resolution. Indeed the inductions are fixed by the inventor of such sort to guarantee a working in linear régime and to have a mass of the device to proportion the weakest possible. The geometric measurements are determined from the laws of basis of the electromagnetism for a position of maximal recovery where the flux and the magnetic inductions in the different active parts of the motor are maximal, and this to avoid the problem of the saturations and to minimize the mass of the motor while imposing some inductions magnetic near of the bends saturation of the characteristic B(H). To this point of working, the linearity of the working is guaranteed. The spreadsheet (Excel) includes 172 calculated element lines. A difficulty is to classify the elements between them and between other to separate the data from the results. The spreadsheet permits to calculate the geometric measurements of the rotor and the stator, of the generating coil, the winding caracteristics, the temperatures in the different active parts of the motor, the losses and the efficiency for different points of working and fashions of control.

On the other hand, the coefficients fixing the shape of wave of the electromotive forces E.m.f. and the leakagecoefficient of flux are not calculated by the analytic method but are determined by finite element simulations and are introduced thereafter in the analytic calculation. This gait simplifies the

dimensionality while offering a sufficient precision to determine the main measurements of the motor [9-12].

An analytic dimensionality program covering all structures of motors studied provides their control static converter, is established therefore from the equations of which we retail the main. The entries of the program are:

- specifications of the electric vehicle.
- properties of the materials.
- configuration (number of magnets and teeth).
- outside and interior diameter of the motor.
- density of current in the coils and voltage of the continuous bus U_{dc}.
- magnetic induction in the air-gap B_e, in the rotor yoke B_{cr} and in the stator yoke B_{cs}.
- switching frequency of the static converter.
- Power transmitted of the generating coil.
- Report of reduction r_d.

The entries 3 and 4 permit to fix the shape of the magnets, the teeth and slots. The surface of a tooth S_d and the middle length of a spire L_{sp} are calculated from the geometric equations.

3. Static Converter Sizing

3.1. Static Converter Structures

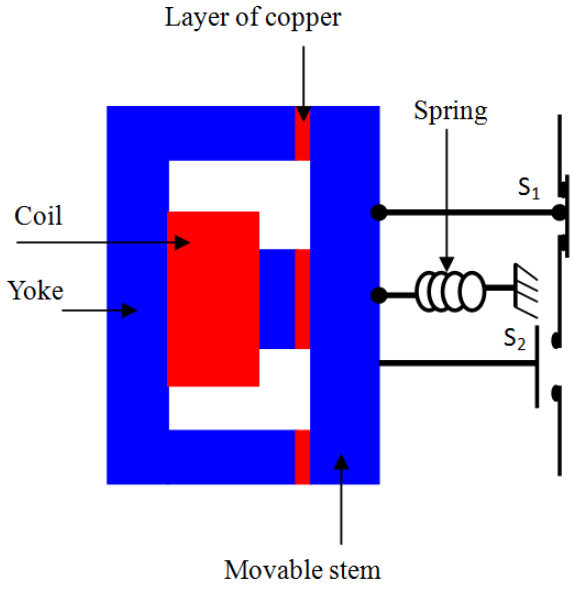

Figure 2. *Arm of the static converter to electromagnetic switches.*

Figure 2 shows an arm of the static converter with electromagnetic switches [6-10].

This structure consists of two mechanical contacts S1 and S2, one normally closed and the other open to avoid the problem of short circuit. The supply of the coil by a sufficient current, causes the attraction of the rod by induction phenomenon, and then the change of state of switches S1 and S2. The excitation coil led to the cancellation of the attraction strength of the stem, allowing switches to resume their initial states.

Another structure without use of the return spring is to cause the moving rod by two generator coils is illustrated in figure 3.

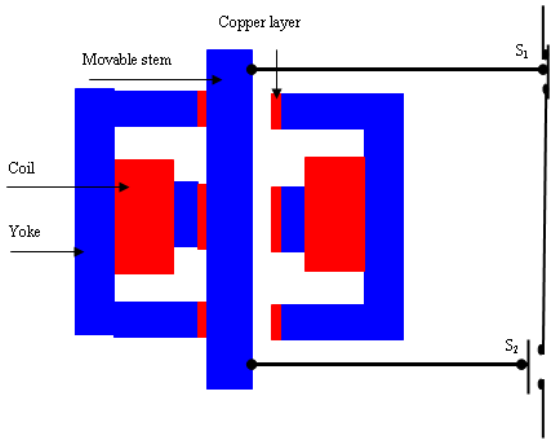

Figure 3. *Inverter arm to two generator coils.*

This structure has the advantage of increasing the switching frequency as that to avoid maintenance problems of springs. This structure may have several floors. It has the disadvantage of a power coil by two complementary voltages.

The design parameters of the generator coil are shown in figure 4.

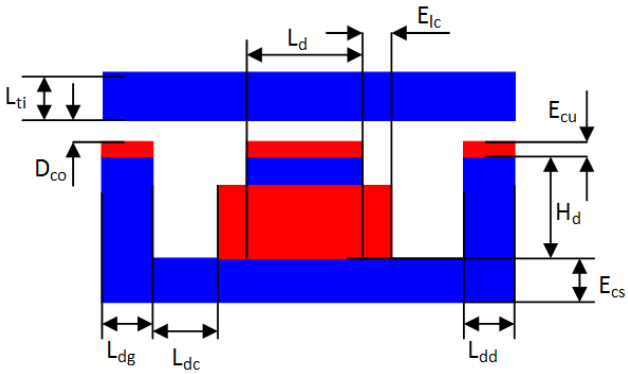

Figure 4. *Design parameters of the generator coil.*

3.2. Generating Winding Sizing

The magnetic induction in the copper when the rod is closed is derived from the application of Ampere's law [6]:

$$B_{ec} = \mu_0 \times \mu_r \times \frac{N_{sb}^2 \times I}{2 \times E_{cu}} \quad (1)$$

Where μ_0 and μ_r are respectively the permeability of air, and the copper (μ_r is very close to 1), N_{sb} is the number of turns of the coil, I is the steady state current of the coil and the E_{cu} is the thickness of copper layer.

The width of the rod is derived from the application of the theorem of conservation of flux between the tooth which is located the coil and the rod [6]:

$$L_{ti} = \frac{B_{ec} \times L_d}{2 \times B_c} \quad (2)$$

Where L_d is the width of the tooth and B_c is the maximum induction in the rod.

The widths of the right and left teeth are given by the following two equations [6]:

$$L_{dg} = \frac{B_{ec} \times L_d}{2 \times B_d} \quad (3)$$

$$L_{dd} = \frac{B_{ec} \times L_d}{2 \times B_d} \quad (4)$$

Where B_d is the induction in the left and right teeth.

The thickness of the yoke is expressed by the following equation [6]:

$$E_{cs} = \frac{B_{ec} \times L_d}{2 \times B_{cs}} \quad (5)$$

Where B_{cs} is the yoke induction.

The section of a main tooth is given by the following relationship [6]:

$$S_d = L_d \times E_b \quad (6)$$

Where E_b is the length of the main tooth (or length of the rod).

The section of the thread depends on the maximum steady-state current (I) and the permissible current density in the copper (δ):

$$S_c = \frac{I}{\delta} \quad (7)$$

The diameter of the conductive wire is given by the following relationship:

$$D_f = \sqrt{\frac{4 \times S_c}{\pi}} \quad (8)$$

The number of conductive layer is deduced by the following relationship:

$$N_{cc} = \frac{H_{db} \times f_{rc}}{D_f} \quad (9)$$

Where f_{rc} is the copper fill factor and H_{db} is the height of the tooth.

The number of copper layer is deduced by the following equation:

$$N_c = \frac{N_{sb}}{N_{cc}} \quad (10)$$

3.3. Modeling of the Electrical Parameters of the Generator Coil

The thickness of the coil is given by the following expression:

$$E_{lc} = N_c \times D_f \quad (11)$$

The average length of a spire is expressed by the following relationship:

$$L_{sp} = 2 \times (L_d + E_b + 2 \times E_{lc}) \quad (12)$$

The resistance of the coil is expressed as follows:

$$R_{bob} = \frac{\rho \times N_s \times L_{sp}}{S_c} \quad (13)$$

Where ρ is the resistivity of copper.

The protection resistance of the coil is used to limit the coil current to the maximum value of the current carried by the coil (I):

(14)

Where U_b is the amplitude of a chopped voltage of coil.

The trajectory of the flux when we energizes the coil is illustrated by the figure 5 [6]:

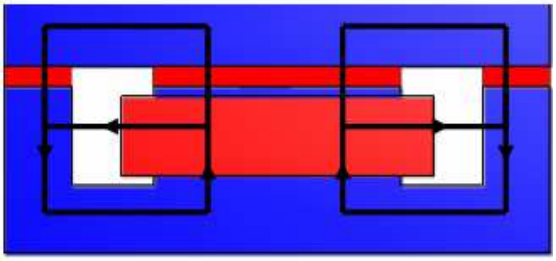

Figure 5. *Path of the field lines to a supply coil.*

Hence, the network reluctance modeling the coil (Figure 6) is deduced:

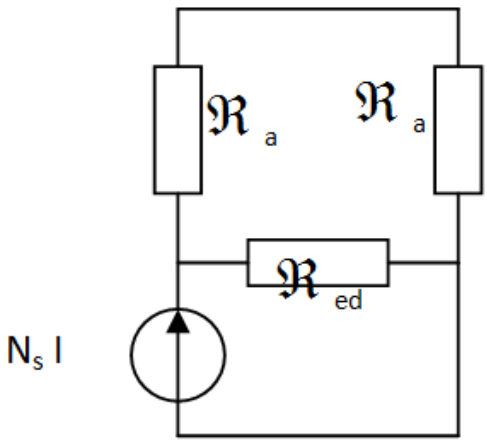

Figure 6. *Network reluctance modeling the coil.*

Where $\Re_a$ is the air-gap reluctance and $\Re_{ed}$ is the reluctance of the space between teeth.

From the network reluctance above we can deduce the

expression of the inductance of the generator coil [6-13]:

$$L_b = \frac{N_{sb}^2}{2\times\Re_a} + \frac{N_{sb}^2}{\Re_{ed}} \quad (15)$$

$$\Re_a = \frac{1}{\mu_0}\times\frac{E_{cu}+D_{co}-x_t}{\frac{S_d}{2}} \quad (16)$$

Where D_{co} is the maximum aperture of the rod and x_t is the displacement of the rod.

$$\Re_{ed} = \frac{1}{\mu_0}\times\frac{E_{lc}+L_{dc}}{H_{cu}\times E_b} \quad (17)$$

Where H_{cu} is the height of the coil and L_{dc} is the distance between the coil and the right tooth.

Hence, the expression of the inductance of the coil is deduced [6-13]:

$$L_b = \mu_0\times N_{sb}^2\times\left(\frac{\frac{S_d}{2}}{2\times(E_{cu}+D_{co}-x_t)}+\frac{H_{cu}\times E_b}{E_{lc}+L_{dc}}\right) \quad (18)$$

3.4. Modelling the Rod Attraction Force

The attraction strength drifts from the energy stocked in the coil:

$$W_b = \frac{1}{2}\times L_b\times I^2 \quad (19)$$

This energy is transformed into mechanical energy on the side of the stem:

$$\frac{dW_b}{dt} = F\times V \quad (20)$$

Where F is the strength of attraction of the stem and V is the speed of the displacement of the stem.

We deducts from (19) and (20):

$$F\times V = \frac{1}{2}\times I^2\times\frac{dL_b}{dx_t}\times\frac{dx_t}{dt} \quad (21)$$

Hence the force of attraction takes the following form:

$$F = \frac{1}{2}\times I^2\times\frac{dL_b}{dx_t} \quad (22)$$

Replacing L_b by his expression, the force of attraction takes the following form [6]:

$$F = \frac{\mu_0\times\mu_r}{4}\times\frac{I^2\times N_{sb}^2}{(E_{cu}+D_{co}-x_t)^2} \quad (23)$$

3.5. Modularity

The electromagnet is a modular structure. Indeed, several modules can be stacked either in series or in parallel to increase the attraction force, and thereafter the opening and closing frequency of the contacts of the static converter.

The series stack of two modules is illustrated in figure 7.

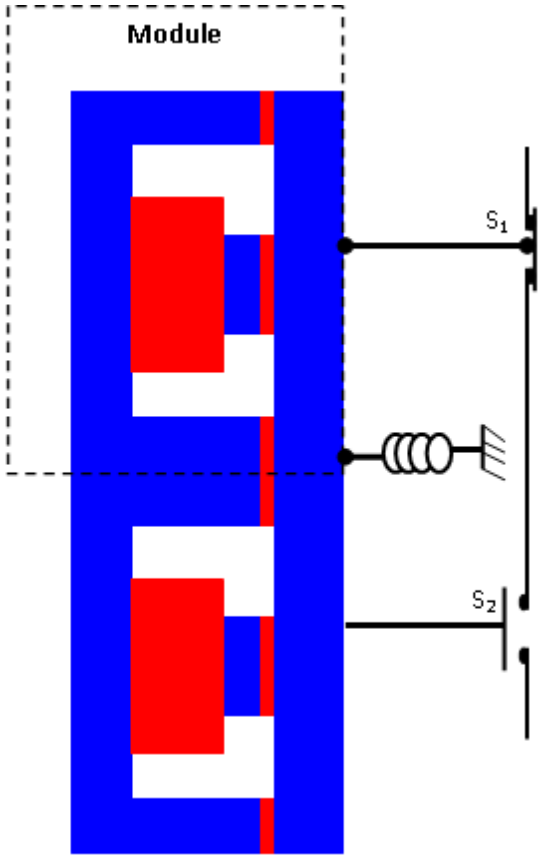

Figure 7. *Stacking in serie of two modules.*

This configuration has the disadvantages of the response time and the maintenance cost of the return spring.

The stack in parallel has the advantage that a frequency of closing and opening of the switches clearly higher in reagard to the stack in series structure, because these actions are performed by action of the attraction force of two generator coils.

The parallel stack of two modules is illustrated in figure 8.

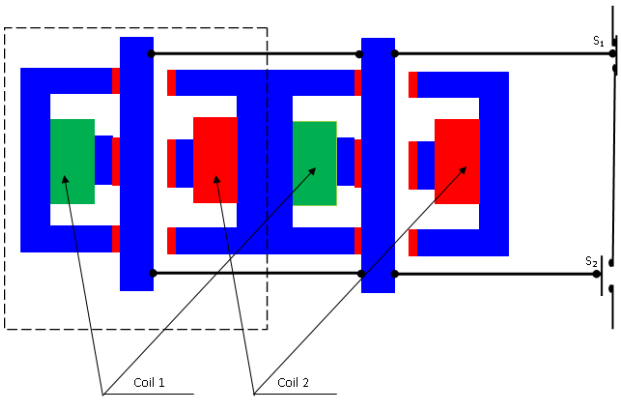

Figure 8. *Stacking in parallel of two modules.*

The equation of movement of the stem is deducted from the fundamental relation of the dynamics [6]:

$$nmp \times M_t \times \frac{dv}{dt} = nmp \times \frac{\mu_0 \times \mu_r}{4} \times \frac{I^2 \times N_{sb}^2}{\left(E_{cu} + D_{co} - x_t\right)^2_t} \quad (24)$$

$$v = \frac{dx_t}{dt} \quad (25)$$

The evolution of the opening time of the mobile core according to the displacement of the stem for a number of module nmp variable of 1 to 5 is illustrated by the figure 9.

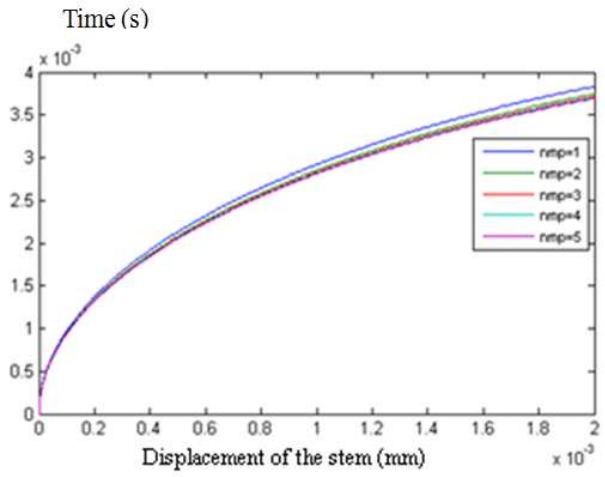

Figure 9. *Evolution of the opening time of the movable core as a function of displacement of the rod for a number of modules nmp ranging from 1 to 5.*

4. Electric Motor Sizing

The magnetic induction in the air gap is calculated for a position of maximum overlap (the edges of a magnet merge with the edges of the main tooth relative to the stator pole), since this position is relative to the maximum induction in the different active parts of the stator magnetic pole of the motor. The distribution of the field lines to this position is illustrated by figure 10.

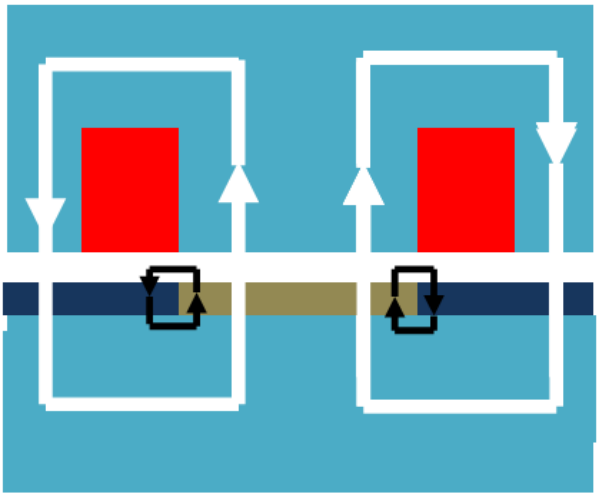

Figure 10. *Distribution of the field lines to a position of maximum recovery.*

This figure shows that the flux is divided into useful flux for the traction of the rotor and leakage flux between the magnets.

Applying Ampere's theorem at stator pole to a supply of the stator coil by the maximum current of the motor, regardless of the magnetic flux due to the magnets, used to calculate the magnetic induction caused by the current.

$$\int_{Lignes\ de\ champ} \overrightarrow{H} \times \overrightarrow{dl} = \frac{N_s}{\frac{N_d}{3}} \times I_{\max} = 2 \times \left(H_{ri} \times H_a + H_{ri} \times e\right) \quad (26)$$

Where I_{max} is the maximal current of the motor, H is the magnetic field, H_{ri} is the magnetic field in the air-gap, H_a is the height of a magnet, e is the thickness of the air-gap, μ_0 is the permeability of air, N_s is the number of spires by phase and N_d is the number of main teeth.

$$B_{ri} = \mu_0 \times H_{ri} \quad (27)$$

Where B_{ri} is the magnetic induction due to the energize of the motor by the maximal current (I_{max}):

$$B_{ri} = \frac{\mu_0}{2 \times \frac{N_d}{3}} \times \frac{N_s \times I_{\max}}{H_a + e} \quad (28)$$

This induction is negligible compared to the induction created by the magnets, since the flux generated by the coil through two times the thickness of the magnets and the air gap having both a very low magnetic permeability. Accordingly, only the magnetic flux generated by the magnets is used for sizing the motor.

This induction is derived from the application of Ampere law on a closed contour of the field lines:

$$\int_{lines\ de\ champ} \overrightarrow{H} \times \overrightarrow{dl} = 0 = 2 \times \left(H_m \times H_a + H_e \times e\right) \quad (29)$$

The magnetic induction in the air gap is linear in function of the magnetic field in the gap:

$$B_e = \mu_0 \times H_e \quad (30)$$

While applying the theorem of conservation of flux to the level of the air-gap, we deduce the expression of the induction in the air-gap according to the induction in the magnets and the coefficient of leakage flux:

$$B_a \times S_a \times K_{fu} = B_e \times S_d \quad (31)$$

The magnetic induction of the magnets takes the following relation:

$$B_a = \frac{S_d}{S_a} \times \frac{B_e}{K_{fu}} \quad (32)$$

The induction in the magnets is approached by the following linear equation:

$$B_a = \mu_0 \times \mu_r \times H_m + B_r \quad (33)$$

Where μ_r is the relative permeability of the magnets and B_r is the residual magnetic induction of magnets.

From the equations (29), (30), (31), (32) and (33), we deducts the height of the magnets imposing an induction in the air-gap B_e. This induction is chosen of a manner to have magnetic inductions in the different active parts of the motor near of the bends saturation of the characteristic B-H, leading to a minimal mass of the motor and a working in the linear regime [10]:

$$H_a = \mu_r \times \frac{B_e}{B_r - \frac{S_d \times B_e}{S_a \times K_{fu}}} \times e \tag{34}$$

Where K_{fu} is the leakages flux coefficient.

To avoid the demagnetization of the magnets, the current of phase must be lower than demagnetization current I_d [10]:

$$I_d = \left(\frac{B_r - B_c}{\mu_r} \times H_a - B_c \times K_{fu} \times e \right) \times \frac{p}{2 \times \mu_0 \times N_s} \tag{35}$$

Where B_c is the demagnetization induction, B_r is the residual induction of magnets and μ_0 is the permeability of air.

The height of the rotor yoke and the stator yoke is derived by application of the theorem of conservation of flux between the magnet and a rotor yoke, and between the stator tooth and the stator yoke [10]:

$$H_{cr} = \frac{B_e}{B_{cr}} \times \frac{Min(S_d, S_a)}{2 \times \left(\frac{D_e - D_i}{2} \right)} \times \frac{1}{K_{fu}} \tag{36}$$

$$H_{cs} = \frac{B_e}{B_{cs}} \times \frac{Min(S_d, S_a)}{2 \times \left(\frac{D_e - D_i}{2} \right)} \tag{37}$$

Where B_{cr} and B_{cs} are respectively the induction in the rotor yoke and in the stator yoke, S_d and S_a are respectively the section of a tooth and the one of a magnet and K_{fu} is the coefficient leakages flux.

5. Finite Element Validation of the Analytic Design Approach

5.1. Finite Element Model

The motor is studied on a cylindrical cut plan. The plan of cut makes itself according to the middle diameter of the motor (Figure 11), then we spreads the structure, that means the length of the cuts L_c is the perimeter of the circle according to the done cut and this next is on the middle diameter. This quantity is worth:

$$L_c = 2 \times \pi \times \left(\frac{D_e + D_i}{4} \right) \tag{38}$$

The width of a main tooth is given by the following relation:

$$L_d = A_{dentm} \times \left(\frac{D_e + D_i}{4} \right) \tag{39}$$

Where A_{dentm} is the middle angle of opening of a main tooth.

The width of a inserted tooth is given by the following relation:

$$L_d = A_{dentim} \times \left(\frac{D_e + D_i}{4} \right) \tag{40}$$

Where A_{dentim} is the middle angle of opening of a inserted tooth.

The slot width is given by the following relation:

$$L_{enc} = \left(\frac{D_e + D_i}{2} \right) \times \sin\left(\frac{1}{2} \times \left(\frac{2 \times \pi}{N_d} - \alpha \times \beta \times \frac{\pi}{p} \times (1 - r_{did}) \right) \right) \tag{41}$$

The width of a magnet is expressed by the following relation:

$$L_d = \frac{\pi}{p} \times \beta \times \left(\frac{D_e + D_i}{4} \right) \tag{42}$$

The length of the model is expressed like follows:

$$L_m = \frac{D_e - D_i}{2} \tag{43}$$

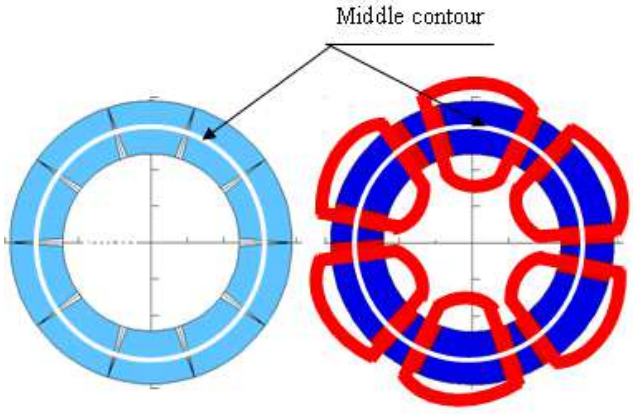

Figure 11. *Contour of the cylindrical cut.*

When we spreads the cylindrical cut plan, we gets the model 2 D of the motor (Figure 12).

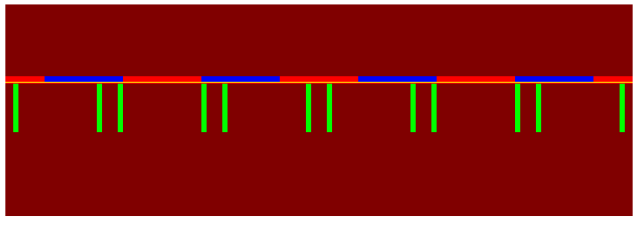

Figure12. *2-D model of the motor.*

5.2. Distribution of the Flux Lines

The flux line at load for the trapez motor and the sinus motor are illutrated respectively by figure 13 and figure 14 [13]:

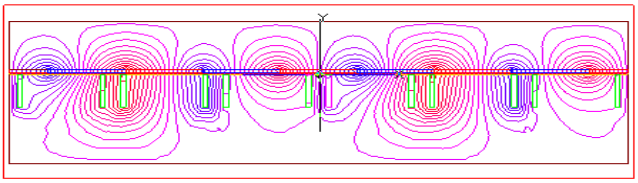

Figure 13. *Distribition of the flux line of trapeze motor.*

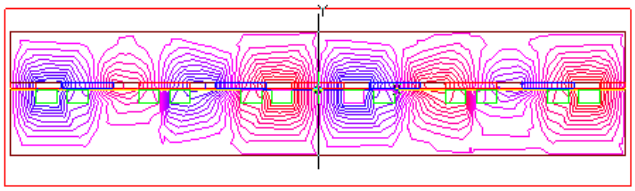

Figure 14. *Distribition of the flux line of sinus motor.*

The distribution of field lines shows that there is no leakage of inter-magnets, which leads to consider the coefficient of leakage flux is equal to 1 (K_{fu}=1). This property is found by optimizing the geometric parameters (e, β et α) by finite element simulations.

The flux at load for the motor with tarpezoïdal wave-form is illustrated by the figure 15[13]:

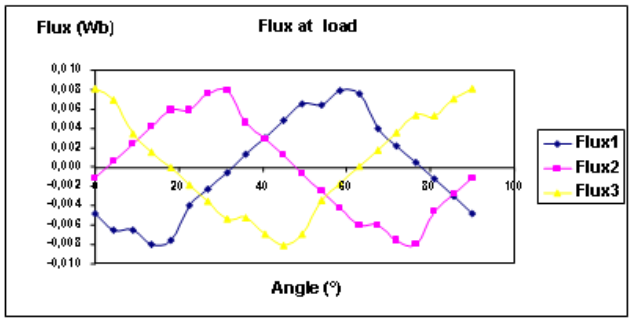

Figure 15. *Flux at load for the motor with tarpezoïdal wave-form.*

The flux at load for the motor with sinusoïdal wave-form is illustrated by the figure 16 [13] :

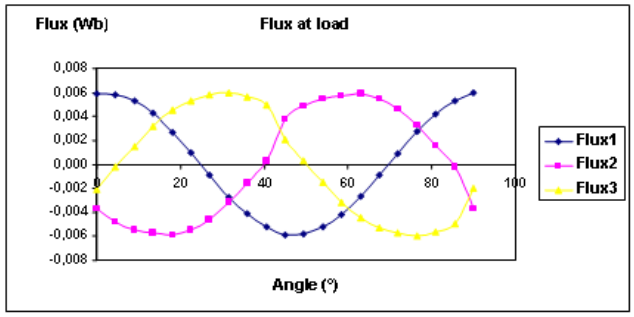

Figure 16. *Flux at load for the motor with sinusoïdal wave-form.*

The electromotive forces (Emf) at load for the motor with Trapezoïdal wave-form is illustrated by the figure 17 [13]:

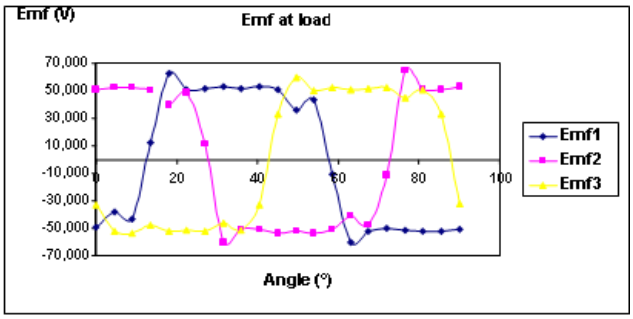

Figure 17. *Emf at load for the motor with trapezoïdal wave-form.*

The electromotive forces at load for the motor with sinusoïdal wave-form is illustrated by the figure 18 [13]:

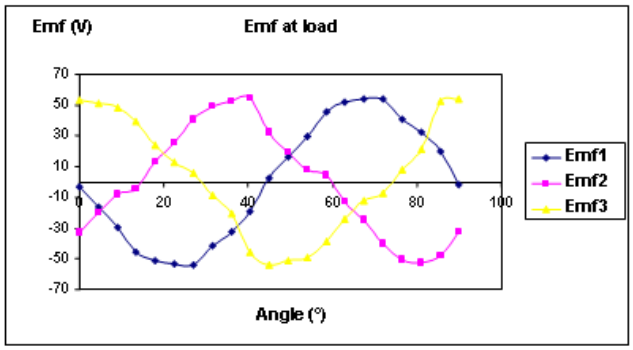

Figure 18. *Emf at load for the motor with sinusoïdal wave-form.*

The values of flux, Emf and torque acheive the these found by analytic calculation, what validates this design approach.

6. Power Chain Global Model

A gobal model with energy recuperation system based on sinusoidal and trapezoidal control is developed and implanted under Malab-Simulink environnement as shown in figure 19 [13]:

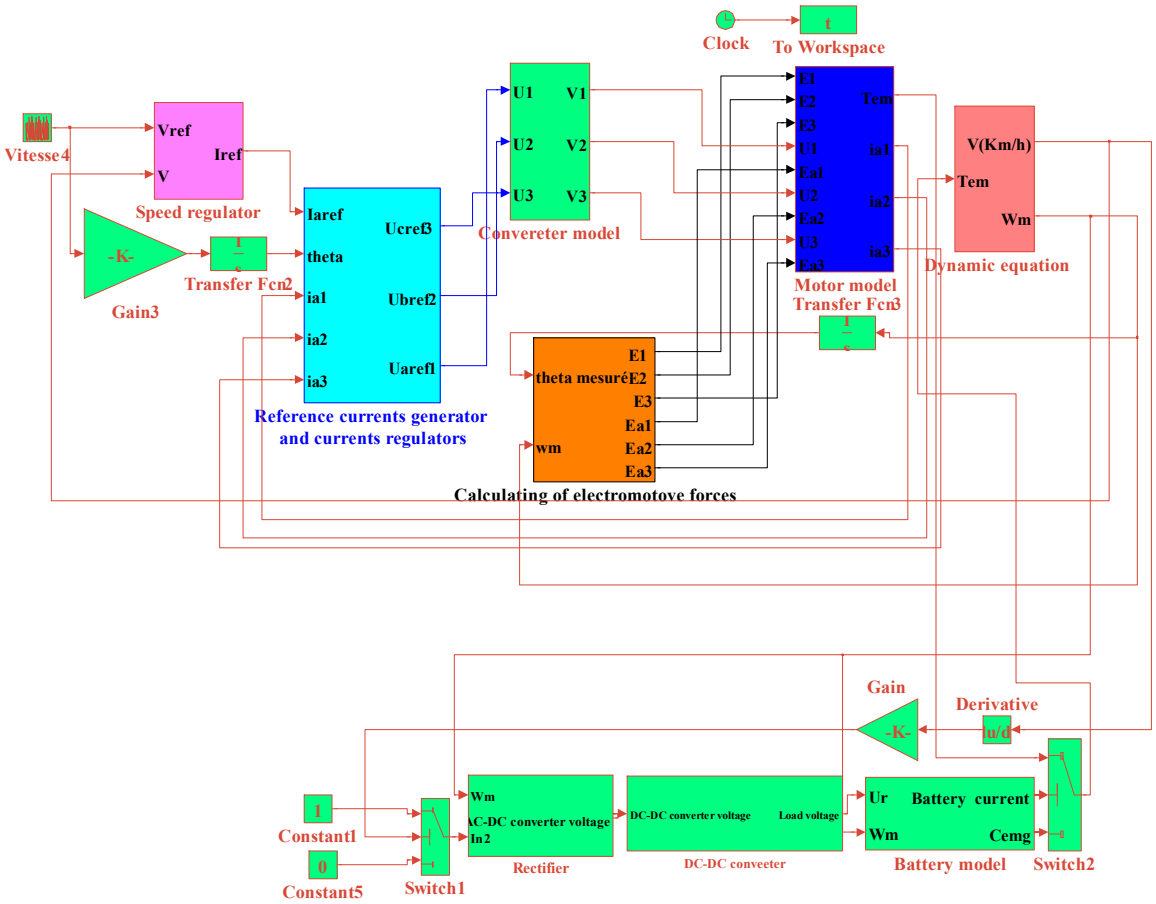

Figure 19. *Global model with energy recuperation system.*

7. Simulations Results

The response of speed to the speed of reference in the two cases is illustrated by the figure 20:

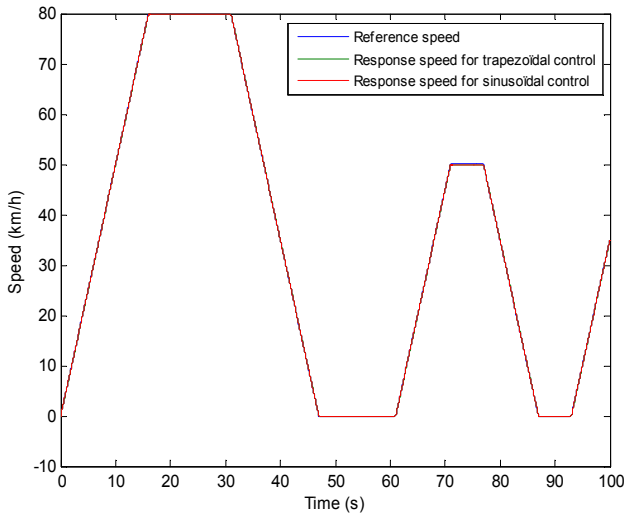

Figure 20. *Speed responses.*

This figure shows the good dynamic characteristic and valid thereafter the approach of design of the two power chains.

The current of phase in the two cases is illustrated by the figure 21:

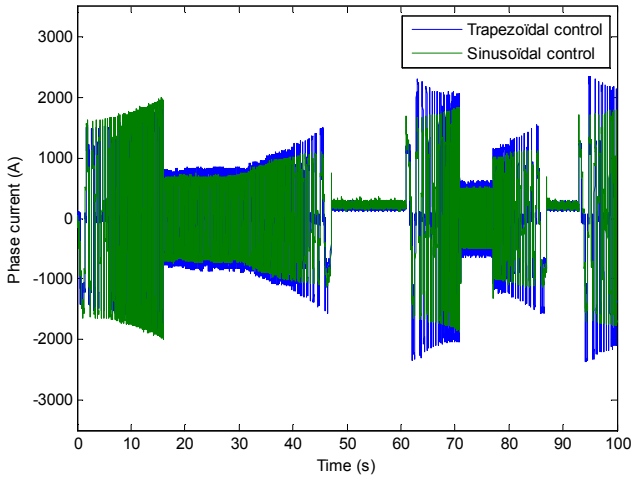

Figure 21. *Phase current.*

This figure shows that the currents are comparable, what proves the setting in equivalence of the two structures of power chains. This face also shows that the current of starting is weak for the two structures what shows the performance of the two chosen control techniques.

The figure 22 illustrates the evolutions of the phase currents for the two power chains:

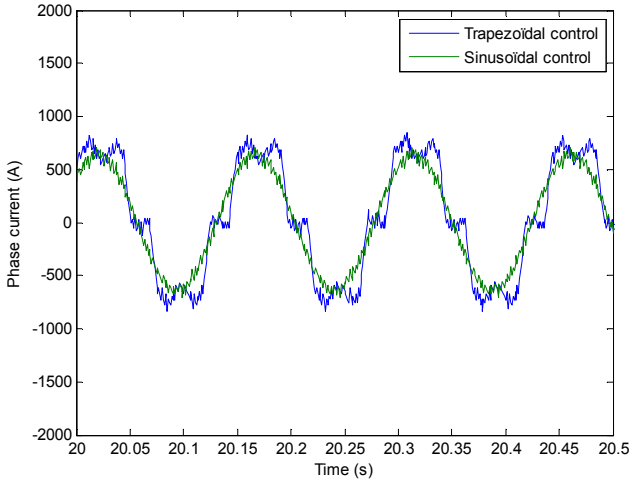

Figure 22. *Evolutions of the phase currents for the two power chains.*

For the trapeze control, the pace of the current is very close to a trapezoidal shape. For the sinus control, the pace of the current is close to a sinusoidal shape. This shows the performance of the two techniques of control chosen.

The figure 23 illustrates the evolutions of the energy recovered in the two cases of configuration:

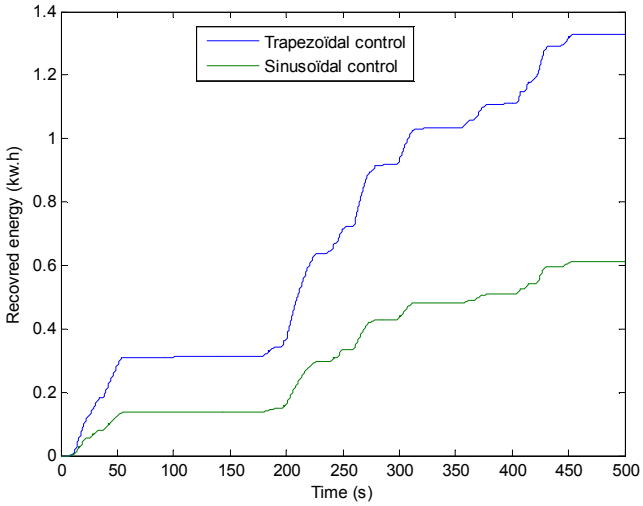

Figure 23. *Recovred energy.*

This figure shows that the energy recovered in the case sinus is distinctly weaker than the one of trapeze case. This energy is of values respectively Ws=0.3276 kw.h and Wt=0.7151 kw.h.

8. Conclusion

In this paper, we present a systematic design tool of EVs power chains based on analytical modeling of design and control parameters of the power chain. This approach takes into account of technological, physical constraints. It is compatible to performance approaches optimization of EVs, such as power to weight ratio, autonomy and reliability. This method provides sufficient accuracy, but is still incomplete since certain coefficients require adjustment, such as coefficient of flux leakage and width of the inserted teeth. In this directive, a validation and complementarity study by the finite element method to adjust the design process is developped and presented. Finally a comparative study between the power chain to trapezoidal control and the other to sinusoidal control is presented. The study of the two power chains performances, following a modelling under the environment of Mtalab/Simulink, watch that these two power chains is comparable and presents an attractive solution for the problem of motorization of the electric vehicles.

References

[1] S. Tounsi, F. Gillon, S. Brisset, P. Brochet et R. Neji: «Design of an axial flux brushless DC motor for electric vehicle», ICEM2002 (15th International Conference on Electrical Machines), 26-28 août à bruges-Belgique, CD: ICEM02-581.

[2] A. AMMOUS, B. ALLARD, H. MOREL: «Transient temperature mesurements and modeling of IGBT's under short circuit», IEEE transaction electronic devices, vol. 13, n° 1, 1998, p. 12-25.

[3] P. BASTIANI : «Stratégies de commande minimisant les pertes d'un ensemble convertisseur machine alternative : application à la traction électrique», Thèse INSA 01 ISAL 0007, 2001

[4] S. TOUNSI, «Modélisation et optimisation de la motorisation et de l'autonomie d'un véhicule électrique», Thèse de Doctorat 2006, ENI Sfax.

[5] S. TOUNSI et R. NEJI: «Design of an Axial Flux Brushless DC Motor with Concentrated Winding for Electric Vehicles», Journal of Electrical Engineering (JEE), Volume 10, 2010 - Edition: 2, pp. 134-146.

[6] S. TOUNSI, M. HADJ KACEM et R. NEJI « Design of Static Converter for Electric Traction », International Review on Modelling and Similations (IREMOS) Volume 3, N. 6, December 2010, pp. 1189-1195.

[7] R. NEJI, S. TOUNSI et F. SELLAMI: «Contribution to the definition of a permanent magnet motor with reduced production cost for the electrical vehicle propulsion», European Transactions on Electrical Power (ETEP), 2006, 16: pp. 437-460.

[8] S. TOUNSI, R. NEJI, and F. SELLAMI: «Design Methodology of Permanent Magnet Motors Improving Performances of Electric Vehicles», International Journal of Modelling and Simulation (IJMS), Volume 29, N° 1, 2009.

[9] R. NEJI, S. TOUNSI, F. SELLAMI: «Optimization and Design for a Radial Flux Permanent Magnet Motor for Electric Vehicle», Journal of Electrical Systems, Volume 1, isuue 4 (2005), pp. 47-68.

[10] S. TOUNSI, « Dimensionnement et modélisation d'un moteur synchrone à flux axial pour la propulsion de véhicule électrique de loisirs » Mémoire de DEA électronique, Ecole Nationale d'Ingénieurs de SFAX - TUNISIE, 2001.

[11] A. MOALLA, S. TOUNSI et R. NEJI: «Determination of axial flux motor electric parameters by the analytic-finite elements method», Journal of Electrical Systems, volume 4, issue 4, 2008, pp. 398-409.

[12] A. MOALLA: «Détermination des Paramètres d'un Moteur Synchrone à Aimants Permanents à Flux Axial » Mémoire de mastère CEER, juillet 2007, Ecole Nationale d'Ingénieurs de Sfax (ENIS).

[13] S. TOUNSI « Comparative study of trapezoïdal and sinusoïdal control of electric vehicle power train», International Journal of Scientific & Technology Research (IJSTR), Vol. 1, Issue 10, Nov 2012.